The impact of solvent tanδ on the magnetic characteristics of nanostructured NiZn-ferrite film deposited by microwave-assisted solvothermal technique

Cite as: AIP Advances **11**, 025003 (2021); https://doi.org/10.1063/9.0000190
Submitted: 28 October 2020 . Accepted: 11 January 2021 . Published Online: 02 February 2021

R. D. Ralandinliu Kahmei, Sarath Arackal, S. A. Shivashankar, Navakanta Bhat, and Ranajit Sai

The impact of solvent tanδ on the magnetic characteristics of nanostructured NiZn-ferrite film deposited by microwave-assisted solvothermal technique

Cite as: AIP Advances 11, 025003 (2021); doi: 10.1063/9.0000190
Presented: 2 November 2020 • Submitted: 28 October 2020 •
Accepted: 11 January 2021 • Published Online: 2 February 2021

R. D. Ralandinliu Kahmei, Sarath Arackal, S. A. Shivashankar, Navakanta Bhat, and Ranajit Sai[a)]

AFFILIATIONS

Centre for Nano Science and Engineering (CeNSE), Indian Institute of Science (IISc), Bengaluru 560012, India

Note: This paper was presented at the 65th Annual Conference on Magnetism and Magnetic Materials.
[a)]**Author to whom correspondence should be addressed:** ranajit@ieee.org

ABSTRACT

Nanostructured Ni-Zn ferrite (NZF) thin films, deposited by a CMOS-compatible microwave-assisted solvothermal deposition (MAS-D) process, exhibit 'far-from-equilibrium' distribution of cations in the spinel structure, and thus, exciting magnetic properties. Solvents with different dielectric loss-tangents, such as ethanol (tanδ≈0.94), 1-decanol (tanδ≈0.1), and benzyl alcohol (tanδ≈0.67), were mixed in five judiciously-chosen proportions – ED35 (ethanol:1-decanol=3:5; tanδ≈0.51), ED33 (tanδ≈0.63), EB25 (tanδ≈0.66), EB35 (tanδ≈0.70), and EB33 (tanδ≈0.74) – to study the impact of effective tanδ on cation occupancy and the nature of magnetization in the resulting films. The maximum temperature attained during microwave irradiation (T_{max}) and the heating rate ($\Delta T/t_{rise}$) increase as the effective tanδ of the solvent mixture increases, which in effect leads the Ni atoms to migrate towards equilibrium lattice sites. Unlike bulk NZF, where all Ni atoms occupy octahedral sites (B-sites), the films reported here exhibit just 28% of Ni atoms in B-sites at best when deposited from the precursor solution EB25. At room temperature all films are superparamagnetic, while the maximum moment (M_S=100 emu/cc) is observed in the film with the highest % of Ni atoms in B-sites. Thermoremanent magnetization (TRM) of the samples is studied and compared. Very high effective anisotropy constants (K_{eff}=140 kJ/m^3), and two-orders-of magnitude-higher inter-particle dipole moment ($E_{dipole}\approx 8\times10^{-20}$ J @300 K) are observed in samples prepared from benzyl alcohol rather than 1-decanol – signifying the potential for tailoring magnetic properties by the choice of solvents in the MAS-D process.

INTRODUCTION

Nickel zinc ferrite (NZF) is one of the most explored soft magnetic materials due to its high saturation magnetization (M_s), high resistivity, high ferromagnetic resonance frequency (f_{FMR}), high permeability (**μ**) and low loss, all of which are vital for high frequency applications.[1–3] Besides vacuum-based deposition techniques NZF films have been deposited by various solution-based techniques such as spin-spray plating, spray pyrolysis, spin coating, sol-gel, and hydrothermal, and used in applications ranging from radio-frequency inductors to electromagnetic noise suppressors.[4–8] Recently, we have developed a CMOS-compatible, low temperature Microwave-Assisted Solvothermal Deposition (MAS-D) process for various spinel ferrites and demonstrated its capability to yield smooth, uniform films with desired crystallite size.[9–11] For example, a soft magnetic NZF thin film was successfully synthesized using ethanol:1-decanol as solvent, and its structural and magnetic properties thoroughly characterized.[10] At 2.45 GHz, the timescale over which the field oscillates is about the same as the relaxation time (τ) of permanent dipoles in most organic and inorganic molecules. So, strongly polarizable solvents are particularly advantageous for rapid heating in MAS-D. Rapid energy transfer directly to the reactants allows instantaneous decomposition of the precursors, creating supersaturated solutions suitable for film

deposition. However, the effect of the dielectric loss tangent of the solvent on physical properties, especially on the magnetic properties, was not studied.

Benzyl alcohol (BA) plays a unique role as reaction medium for synthesizing metal oxide nanoparticles as well as oxide-based organic-inorganic hybrids. It is a mildly co-ordinating agent with high boiling point (BP 205 °C) and tanδ=0.667. Although it is relatively a bulky molecule, its τ in the microwave field is not much longer than that of ethanol (EA, tanδ=0.941), probably due to the localized rotation of the CH_2OH group rather than whole-molecule rotation.[12] In contrast, ethanol is a weak co-ordinating solvent with a lower BP (78 °C), normally used both to homogenize the reaction medium and initiate chemical reaction-generating hot spots.[13,14] Jena *et al.* reported that BA allowed the formation of monodispersed TiO_2 nanoparticles (7 nm), whereas EA yielded randomly-oriented and densely-packed nanocrystals (100-400 nm).[15] In contrast, 1-Decanol (D, tanδ~0.1) behaves as a heat sink, since it does not couple efficiently with microwave radiation. When combined with a highly polar solvent like EA, the heat produced from the polar reagents under microwave irradiation will be drawn away, keeping the temperature low, while allowing reaction(s) to receive activation energy. Therefore, given its high tanδ, EA accelerates reactions, leading to rapid formation of nuclei and their uncontrolled growth, while D or BA serves as a capping agent and/or heat sink, controlling size but providing high crystallinity. Growing a densely-packed nano (poly)crystalline ferrite film for on-chip inductors and other devices is a challenge, since structural parameters directly influence intrinsic electrical and magnetic properties.

The combination of EA and BA or D with "microwave chemistry" can provide a controlled, versatile reaction system tunable for various applications. Via the MAS-D process, we explored the impact of solution tanδ on the structure of the spinel nanocrystallites, and thus, on the magnetic properties of the various NZF films deposited on Si (100) substrates by using precursor solutions with various volume ratios of EA, BA, and D as solvents.

EXPERIMENTAL

In a typical MAS-D process, selected metal precursors dissolved in a chosen high-tanδ solvent mixture transform into metal oxide under microwave irradiation and nucleate on an immersed substrate. Metalorganic precursors are desirable for oxide synthesis due to their low susceptibility to hydrolysis and low moisture sensitivity. Ni(II)acac, Zn(II)acac and Fe(III)acac were used as precursors (0.5:0.5:2 molar ratio; acac=acetylacetonate), and AR-grade ethanol (EA), 1-decanol (D), and benzyl alcohol (BA) were used as solvents

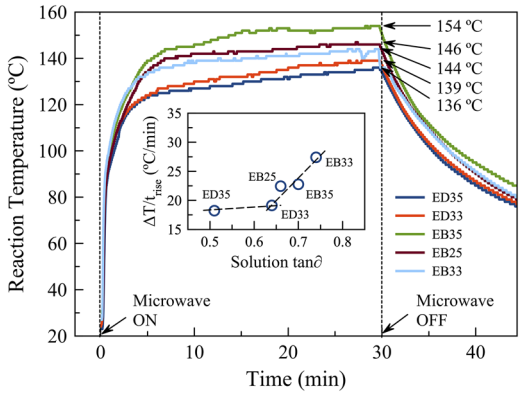

Fig. 1. Heating profile of the precursor solutions used for the deposition of NZF by MAS process, with inset showing the rate of change of temperature during heating to be directly proportional to tanδ.

to prepare various reaction mixtures (volume ratio of EA:D=3:5 (ED35), EA:D=3:3 (ED33), EA:BA=2:5 (EB25), EA:BA=3:5 (EB35), and EA:BA=3:3 (EB33), with ED35 reported earlier.[10] The tanδ ($= \varepsilon_r''/\varepsilon_r'$) of each solution was measured at 300 K at 2.45 GHz (the operating frequency of the microwave reactor used in MAS-D process) by a coaxial dielectric probe kit (Performance Probe, Keysight Inc.) connected to a vector network analyser and is tabulated in Table I. NZF films were deposited on a 1 cm × 1 cm Si (100) by exposing 10 ml of each reaction mixture with a constant microwave power (300 W) for 30 mins. The deposited films are named after the respective precursor solution mixture. Figure 1 shows the temperature-time profile of the as-prepared solutions, with the inset showing that the rate of increase of temperature ($\Delta T/t_{rise}$) increases with increase in tanδ – more so in presence of benzyl alcohol. Supersaturation was attained within 50 s, initiating nucleation on the immersed substrate, followed by film growth. The substrate was taken out after cooling the solution, sonicated twice in ethanol to remove loose particles lying on the film, and dried (55 °C, 1 hr) in air. All the samples were prepared under identical microwave-exposure and post-exposure treatment protocols, with the solvent compositions of the reacting solution being the only difference. The maximum process temperatures attained in each case were also tabulated in Table I.

The crystal structure of the films was characterized by X-ray diffractometry (XRD) (Rigaku SmartLab, Cu-K_α radiation). Film

TABLE I. The process conditions and the resulting film characteristics of five film samples under study.

Sample code	Measured solution tanδ	$\Delta T/t_{rise}$ (°C/min)	T_{max} (°C)	Chemical formula along with Cation distribution	$Ni^{2+}{}_{B\text{-site}}$ (x)	D_{Sch} (nm)	Film thickness 't' (nm)
ED35	0.51	18.2	136	$(Ni_{0.42}Zn_{0.24}Fe_{0.34})[Ni_{0.08}Zn_{0.26}Fe_{1.66}]O_4$	0.08	5.9	190
ED33	0.64	19.1	139	$(Ni_{0.43}Zn_{0.16}Fe_{0.41})[Ni_{0.07}Zn_{0.34}Fe_{1.59}]O_4$	0.07	7.2	219
EB25	0.66	22.2	146	$(Ni_{0.36}Zn_{0.27}Fe_{0.37})[Ni_{0.14}Zn_{0.23}Fe_{1.63}]O_4$	0.14	7.9	216
EB35	0.70	22.8	154	$(Ni_{0.37}Zn_{0.20}Fe_{0.43})[Ni_{0.13}Zn_{0.30}Fe_{1.57}]O_4$	0.13	6.1	150
EB33	0.74	27.4	144	$(Ni_{0.39}Zn_{0.17}Fe_{0.45})[Ni_{0.11}Zn_{0.33}Fe_{1.55}]O_4$	0.11	6.0	66

thickness, morphology, and roughness were analysed by scanning electron microscopy (SEM) (Zeiss – Ultra 55) and atomic force microscopy (AFM) (Park NX20). Atomic arrangements in the crystal of all film samples were quantitatively analysed by deconvoluting Raman-modes obtained with a 532 nm laser and a CCD detector (Horiba LabRam HR). DC magnetic measurements were made using a superconducting quantum interference device (SQUID) (Quantum Design. MPMS 3).

RESULTS AND DISCUSSION

The XRD patterns (Fig. 2(a-e)) show crystalline cubic spinel phases, with average crystallite size of ~6 to 8 nm in all samples (fitting characteristics and size determination explained in supplementary material, section S1). FESEM and AFM (Fig. 2(f-t)) show densely packed films, thickness ~ 200 nm, the surface roughness increasing from 1.2 nm to >10 nm with increasing tanδ (Table I). This is due to the high $\Delta T/t_{rise}$, which triggers higher reaction rates leading to slightly less uniform film growth.

MAS-D process is well known for its kinetically driven crystal growth, which leads to far-from-equilibrium cation distribution inside the spinel structure of the nanocrystalline ferrite films.[16,17] The distribution of cations in the NZF lattice was examined by Raman spectroscopy. The spinel structure (space group Fd-3m) exhibits five Raman active modes: A_{1g}, E_g, and T_{2g} (1, 2 and 3) owing to the symmetric and asymmetric bending or stretching of oxygen ions bonded with the metal ions.[18] Raman spectra of the samples with their modes are shown in Fig. 3(a-e).

The A_{1g} peak represents the symmetric stretch in the A-site (tetrahedral) wherein different metal–oxygen stretches appear at different wavenumbers due to mass difference. Broadening of the A_{1g} peak indicates the occurrence of multiple cations in the A-site, with lighter ions responding at higher wavenumbers and heavier ions at lower wavenumbers.[19] The A_{1g} peaks of the samples were deconvoluted by fitting them with individual Lorentzian components to identify cation occupancy in the A-site. The integrated intensity of A_{1g} mode is proportional to the $Ni_{A\text{-site}}$, $Fe_{A\text{-site}}$, and $Zn_{A\text{-site}}$ content in the A-site.[19] The cation occupancy in the A- and B-sites was estimated from the area under the deconvoluted peaks (Table I).

It is seen that there is a significant reduction in Ni^{2+} concentration in B-site of all samples with respect to the bulk values (as marked by the dashed red line in Fig. 3(f)) – attesting to the presence of far-from-equilibrium cation distribution in the film deposited by the MAS-D process. Among the samples obtained from 1-decanol containing solutions, ED35 and ED33, decreasing vol% of 1-decanol increases the tanδ of the solution, but does not have much impact on the cation distribution. In samples obtained from benzyl alcohol containing solutions – EB25, EB35, and EB33 – decreasing vol% of benzyl alcohol, in contrast, decreases B-site occupancy of the Ni^{2+} ions as well as the tanδ of the solution (shown in Fig. 3(f)). This observation can be explained as follows: In bulk NZF at thermodynamic equilibrium, A-sites are exclusively occupied by Zn^{2+} ions

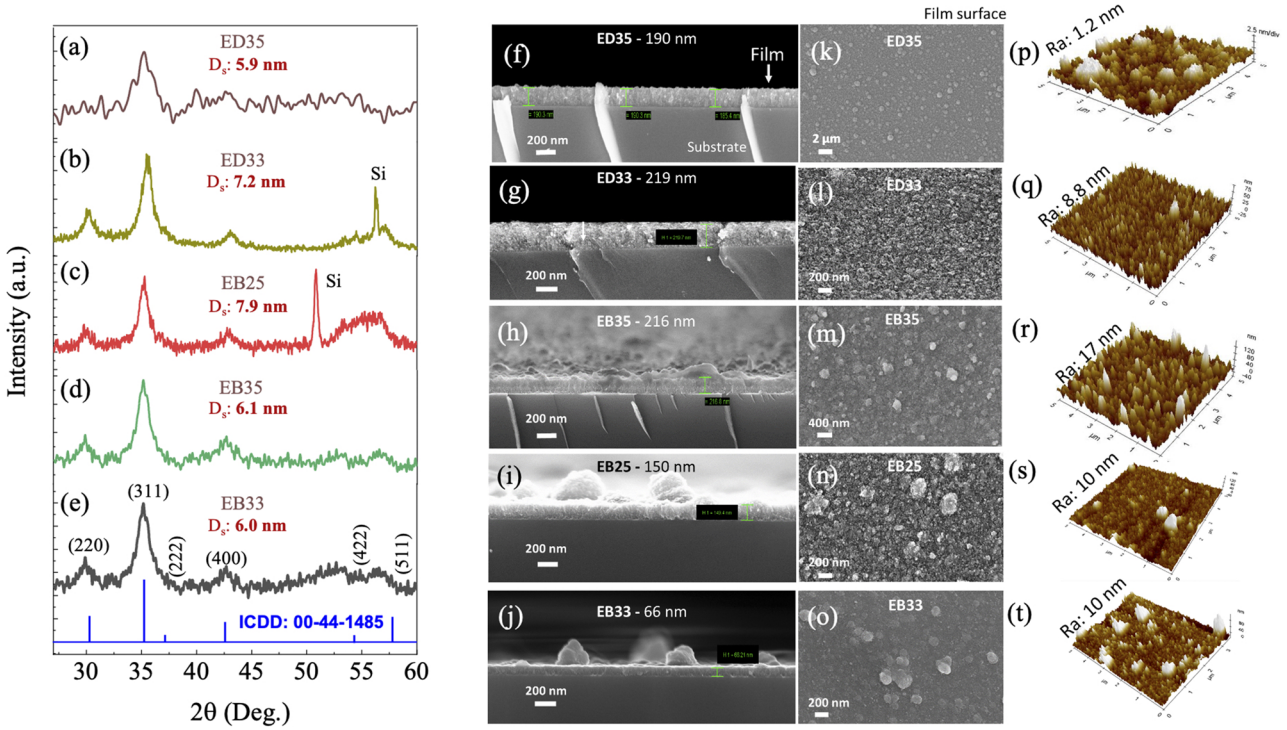

Fig. 2. X-Ray diffractogram of NZF thin films for various tanδ (a-e); FESEM of the films – cross-sectional view (f-j) and film surface morphology (k-o); AFM images (p-t) with average surface roughness (Ra).

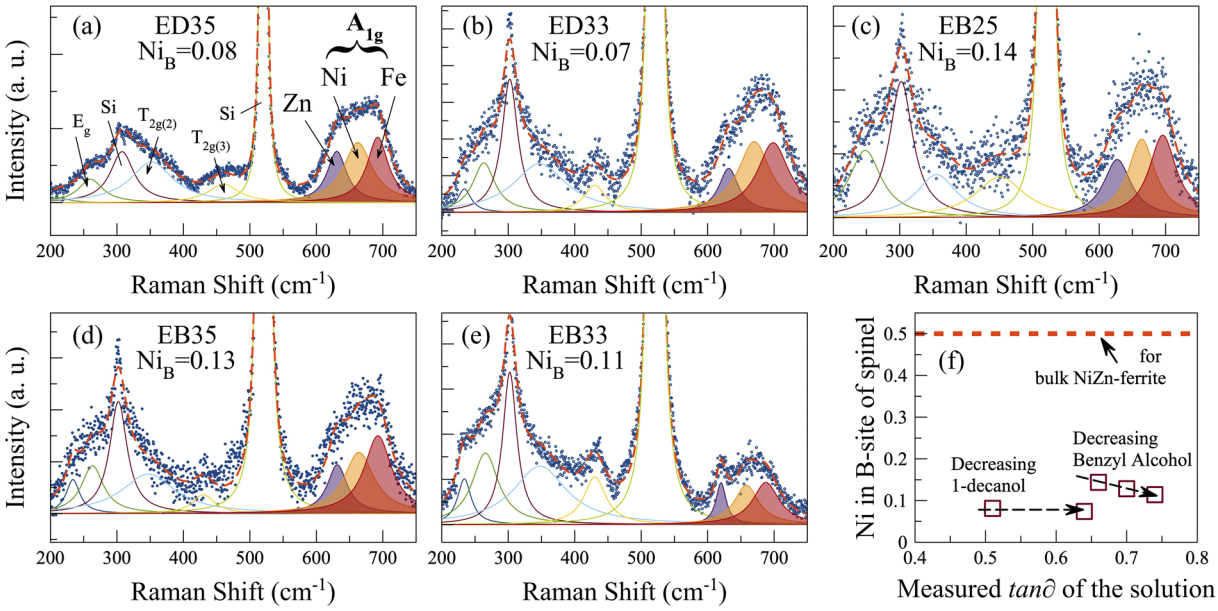

Fig. 3. De-convoluted Raman spectrum of Ni-Zn ferrite thin films (a) ED35 (b) ED33, (c) EB25, (d) EB35, and (e) EB33; (f) Ni^{2+} occupancy in B-site *versus* tanδ.

and B-sites by Ni^{2+}, with Fe^{3+} ions distributed in both A- and B-sites.[20] Annealing at high temperature (~1200°C) or long-duration heating is needed to reach this equilibrium cation distribution. The (somewhat) higher temperature enhances the reactivity of BA due to the endothermic nature of carbon-oxygen dissociative reaction.[21] Here, higher T_{max} induces cations to migrate to thermodynamically more favourable sites, with Ni^{2+} concentration in A-site getting reduced while concentration at the B-site increased. The higher the tanδ, the higher the T_{max} and the heating rate, leading the Ni^{2+} to migrate to more favourable site. In this sense, solvent tanδ in MAS offers effective tunability of cation distribution in the crystal lattice, and thus, of magnetic characteristics.

Field-dependent magnetization (M-H) was measured at 300 K and 5 K (as tabulated in Table II) to study the impact of tanδ on magnetic properties (plots are presented in the supplementary material, section S2). Both at 300 K and 5 K, two clusters of M_s are observed (Fig. 4(a)) – a lower value for samples prepared in 1-decanol-containing solutions than for the benzyl alcohol-containing solutions. High tanδ and high heating rate in benzyl alcohol-containing solutions led to cation distribution in the deposited film closer to the thermodynamically 'equilibrium' state, which in turn, is one of the reasons for the higher Ms (~100 emu/cc at 300 K) in EB25, EB35, and EB33, than (~40 emu/cc) in ED35 and ED33, despite near-identical crystallite sizes (Table I).

All M_s are less than in the bulk, indicative of the finite size and spin-canting effect of the nanoparticles. Using the equation given by Ojha *et al.*,[22] the thickness of the non-magnetic layer caused by surface spin canting (t_{Cant}) was estimated for all samples and tabulated in Table II. Surface disorder at 300 K is as thick as ~1 nm in all samples, implying similar surface effects in the crystallites of all NZF films deposited by MAS-D.

An upturn in magnetization at 5 K (Fig. 4(a)) deviates from modified Bloch's law, where an exponential decay of M_s at low temperatures is expected.[23] Similar behaviour was observed by Maaz *et al.* and Mandal *et al.* (for <50 K), attributed to the effect of surface spin shell moments and quantization of spin-wave spectrum because of finite size.[24,25] The hike in H_c value at 5 K is driven by surface spin-freezing, wherein magnetic moments are

TABLE II. Processing, structural, and magnetic characteristics of various NZF films under study.

Sample	M_s (emu/cc)		H_c (Oe)					
Code	300 K	5 K	300 K	5 K	t_{cant} (nm)	T_B shift (K)	K_{eff} (kJ/m^3)	E_{dipole} ($\times 10^{-22}$ J)
ED35	31	91	29	280	0.96	28	65.1	5
ED33	40	97	11	426	1.13	25	98.2	54
EB25	100	205	265	315	1.09	70	116.1	6880
EB35	89	201	41	108	0.87	86	135.2	2440
EB33	90	276	38	115	0.86	33	140.7	837

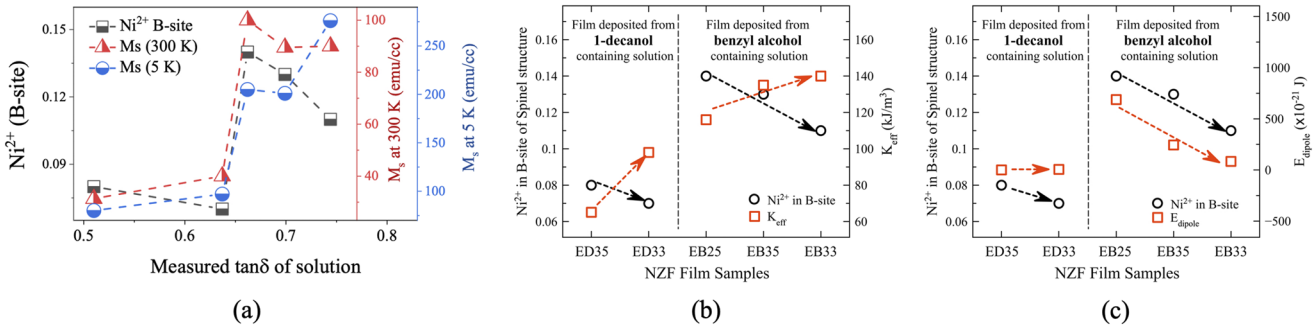

Fig. 4. (a) Dependence of inversion (Ni^{2+} in B-site) and saturation magnetization (M_s) on solution tanδ; Effect of inversion on (b) effective anisotropy constant, and (c) dipole energy.

frozen into anisotropic directions at low temperature. For particles small enough (high surface-to-volume ratio), the inter-particle surface-interaction (among canted spins) can become quite effective, resulting in magnetic hardening or augmentation of H_c. These interactions are rather weak, occurring only at very low temperature.

The far-from-equilibrium cationic distribution is bound to affect the magnetic anisotropy of the NZF films. To investigate the impact, the effective magnetic anisotropy constant (K_{eff}) of each NZF film was determined by fitting the experimental M-H data at the high field using the law of approach to saturation (LAS) given below:[26,27]

$$M(T) = M_s\left(1 - \frac{a}{H} - \frac{b}{H^2}\right) + cH \quad (1)$$

$$b = \left(\frac{8}{105}\right)\left(\frac{K_{eff}}{M_s}\right)^2 \quad (2)$$

where a/H considers the microstructural defects and non-magnetic inclusions, if any, c is associated with magnetic susceptibility at high fields, and b/H2 corresponds to magnetic anisotropy of the material. The detailed methodology of the fitting is provided in the supplementary material,. Since the cationic distribution in all the samples deviates significantly from their bulk counterpart, the contribution of the a/H factor is found to be non-negligible for a good fit. The effective anisotropy constant K_{eff} is calculated using Eq. (2) and the calculated values are presented in Table II.

Fig. 4(b) shows the profound effect of cationic distribution on the effective anisotropy illustrated separately for NZF films deposited from solutions containing 1-decanol and benzyl alcohol. In both cases, as the cationic arrangement in the crystal lattice deviates further away from the equilibrium condition (marked by black arrows), effective anisotropy escalates (marked by red arrows). This observation indicates the rise of a plausible asymmetric local structure inside the symmetric and cubic NZF spinel as the cationic distribution deviates from the equilibrium positions, thereby resulting in greater effective magnetocrystalline anisotropy.

Temperature-dependent zero field cooling (ZFC) and field cooling (FC) measurements were made at 50 and 500 Oe external bias fields to investigate the presence of interparticular interactions in various NZF films, if any. The maximum of the ZFC curve represents the blocking temperature (T_B) of nanoparticles; however, T_B of individual nanoparticles is hidden in the collective behaviour, suggesting strong interaction, as reflected by the wide maxima of ZFC curves (Fig. 5 and supplementary material, S4). ZFC peak-broadening occurs when the effect of inter-particle interaction opposes thermal energy.[28] Furthermore, the interacting system is confirmed by the shift in T_B corresponding to the change in bias field from 50 to 500 Oe in all NZF films. The T_B shift at different fields is a clear indication of dipolar interaction among the nanoparticles. The energy of the dipole-dipole interactions for the NZF films

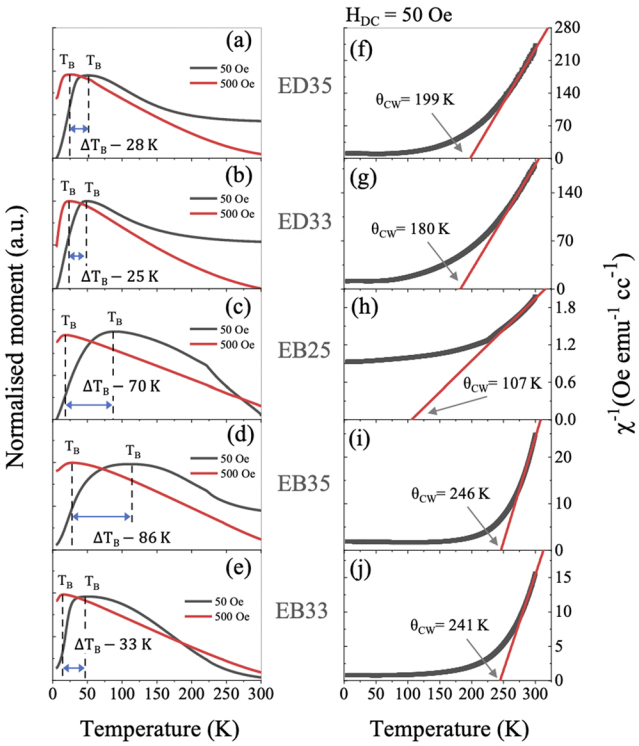

Fig. 5. (a-e) Zero field cooling (ZFC) curve (normalized) measured with the DC bias field of 50 Oe and 500 Oe, and (f-j) temperature-dependent inverse susceptibility plot at 50 Oe bias field.

was approximated by:[29]

$$E_{dipole} \approx \frac{\mu_o \mu^2}{4\pi d^3} \quad (3)$$

where μ ($M_s \times V$) is the magnetic moment and d is average separation. The calculated E_{dipole} of each film is tabulated in Table II and is plotted in Fig. 4(c). Films, deposited in benzyl alcohol-containing solutions having higher tanδ than 1-decanol-containing solutions, exhibit higher M_s and larger T_B shift (Table II), which, in turn, results in a stronger dipolar interactions as presented in Fig. 4(c).

The inverse magnetic susceptibility curve (Fig. 5(f-j) shows the nature of interparticle interaction. The Curie-Weiss paramagnetic temperature (θ_{CW}) occurs in a different temperature region, suggesting a gradual transition in magnetic behaviour. The transition temperature range (where superparamagnetic-to-paramagnetic transition takes place by thermal energy overcoming interparticle interaction completely) is clearly higher in all samples deposited in benzyl alcohol-containing solutions than that in 1-decanol-containing solutions, with the exception of EB25. Néel posited that χ^{-1}becomes nonlinear when magnetic coupling exists between atomic moments and the crystalline lattice.[30] Here, it is also plausible that the gradual transition of the superparamagnetic moment resulted from reasonably short-range magnetic ordering owing to the extreme crystallographic inversion observed in all the MAS-D deposited films.

To further understand the association of K_{eff} and magnetic interaction in films deposited by MAS-D, an estimation of the anisotropy energy distribution (ΔE_B) for EB35 was done by TRM measurement. At first, the sample EB35 was cooled from 300 K to 5 K under a magnetic field of 100 Oe. Under the applied field, the moments magnetize along the field direction and remain magnetized as the temperature decreased to 5 K. After turning off the field, the remnant magnetization (M_{TRM}) was measured while increasing the temperature to 300 K (Fig. 6). The gradual decay in magnetization with increasing temperature implies thermal activation energy (k_BT) overcoming the anisotropy energy barrier (KV), leading to random reorientation and flipping of moments (paramagnetic behavior). The decreasing M_{TRM} reaches a constant value at ~90 K. If all the nanoparticles are superparamagnetic, M_{TRM} should fall to zero, but it is about 2.3 emu/cc here, indicating some blocked nanoparticles even at ~90 to 100 K,[31] attributable to the influence of both magnetic interactions and surface spin effect among the nanoparticles. For non-interacting nanoparticles, the derivative of M_{TRM}, f (T) = -dM_{TRM}/dT gives information on the effective ΔE_B but, because of the presence of interparticle interactions, it only gives a rough estimation of ΔE_B. The broadening of dM_{TRM}/dT peak corresponds to the ΔE_B, accounting for the contribution of interaction energy. In the same vein, Dormann *et al.*[32] reported a progressive increase of ΔE_B with interparticle interaction. For a sufficiently strongly interacting magnetic film like EB35, it is no longer possible to define anisotropy energy of a single particle, rather a wide ΔE_B originating from the assembly of interacting nanoparticles, where a reversal of one particle moment influences others, modifying the energy barrier.

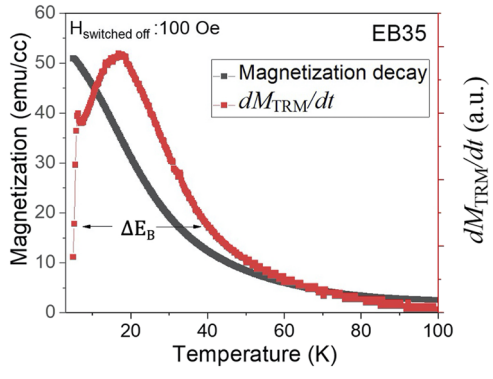

Fig. 6. Magnetization decay curve of NZF film (EB35).

CONCLUSION

Metal-organic precursor solutions of five different dielectric loss-tangent (tanδ) were prepared by mixing solvents of different tanδ in varied proportions. The aforesaid precursor solutions were used to deposit NZF ferrite thin films via a low-temperature CMOS-compatible MAS-D process and the impact of solution tanδ on structural and magnetic properties was investigated. The impact of varying tanδ is reflected in the heating rate ($\Delta T/t_{rise}$) of the precursor solution via dielectric heating and overall process temperature. The films are ~200 nm thick, comprising 6-8 nm crystallites, and exhibit smooth surface. With only 28% of Ni^{2+} ions in octahedral B-sites of the NZF spinel lattice instead of 100% as in bulk, the distribution of the cations is found to be 'far-from-equilibrium' in all films owing to the kinetically driven crystallite formation in MAS-D process. The closer the cationic distribution to the equilibrium condition the higher the M_s and interparticular dipolar interaction. However, the effective anisotropy increases as the cationic distribution deviates from the equilibrium state and exhibits the highest value of ~140 kJ/m^3. Therefore, an interesting trend is observed: increasing tanδ of the precursor solution drives cations to their thermodynamically favourable lattice sites – thus providing a tool for tailoring cationic arrangements and magnetic properties of ferrite films deposited by the MAS-D process. The capability of high tanδ solvents to tailor the degree of inversion and enhance the effective anisotropy could possibly lead to high FMR frequencies suitable for high frequency applications.

SUPPLEMENTARY MATERIAL

Four supplementary material sections exhibits – (1) Deconvolution protocol of the glancing angle X-ray diffractogram to calculate crystallite sizes, (2) M vs. H plots measured at 300 K and 5 K, (3) LAS fit for high-field magnetization, and (4) Temperature dependent magnetization plots under dc bias field of 50 Oe and 500 Oe.

AUTHORS' CONTRIBUTION

All authors contributed equally to this work.

ACKNOWLEDGMENTS

The authors thank MNCF, CeNSE (supported by MHRD, Govt. of India), and Solid State and Structural Chemistry Unit, IISc, for

the instrumentation facilities, and Indian Space Research Organization (ISRO) (Grant Ref.: ISRO/RES-CeNSE-0132) for financial support.

DATA AVAILABILITY

The data that support the findings of this study are available within the article.

REFERENCES

[1]H. P. J. Wijn, M. Gevers, and C. M. van der Burgt, Rev. Mod. Phys. **25**, 91 (1953).
[2]V. G. Harris, A. Geiler, Y. Chen, S. D. Yoon, M. Wu, A. Yang, Z. Chen, P. He, P. V. Parimi, X. Zuo, C. E. Patton, M. Abe, O. Acher, and C. Vittoria, J. Magn. Magn. Mater. **321**, 2035 (2009).
[3]K. Kondo, T. Chiba, H. Ono, S. Yoshida, Y. Shimada, N. Matsushita, and M. Abe, J. Appl. Phys. **93**, 7130 (2003).
[4]N. Matsushita, S. Hatanaka, and M. Abe, IEEE Trans. Magn. **40**, 2011 (2004).
[5]O. Obi, M. Liu, J. Lou, S. Stoute, X. Xing, N. X. Sun, J. Warzywoda, A. Sacco, D. E. Oates, and G. F. Dionne, J. Appl. Phys. **109**, 07E527 (2011).
[6]A. Takayama, M. Okuya, and S. Kaneko, Solid State Ionics **172**, 257 (2004).
[7]Y. Yusuf, R. S. Azis, S. Kanagesan, and G. Bahmanrokh, J. Aust. Ceram. Soc. **53**, 767 (2017).
[8]M. Rivero, A. Del Campo, Á. Mayoral, E. Mazario, J. Sánchez-Marcos, and A. Muñoz-Bonilla, RSC Adv **6**, 40067 (2016).
[9]R. Sai, S. D. Kulkarni, M. Yamaguchi, N. Bhat, and S. A. Shivashankar, IEEE Magn. Lett. **8**, 3703904 (2017).
[10]R. R. Kahmei, R. Sai, S. Arackal, S. A. Shivashankar, and N. Bhat, IEEE Magn. Lett. **10**, 7106005 (2019).
[11]R. Sai, R. D. Ralandinliu Kahmei, S. A. Shivashankar, and M. Yamaguchi, IEEE Trans. Magn. **55**, 2801304 (2019).
[12]N. Pinna, M. Karmaoui, and M.-G. Willinger, J. Sol-Gel Sci. Technol. **57**, 323 (2011).
[13]G. Brătulescu, Y. Le Bigot, and M. Delmas, Synth. Commun. **30**, 171 (2000).
[14]M. Baghbanzadeh, L. Carbone, P. D. Cozzoli, and C. O. Kappe, Angew. Chem. Int. Ed. Engl. **50**, 11312 (2011).
[15]A. Jena, R. Vinu, S. A. Shivashankar, and G. Madras, Ind. Eng. Chem. Res. **49**, 9636 (2010).
[16]R. Sai, S. D. Kulkarni, S. S. M. Bhat, N. G. Sundaram, N. Bhat, and S. A. Shivashankar, RSC Adv **5**, 10267 (2015).
[17]R. Sai, S. Arackal, R. D. R. Kahmei, N. Bhat, M. Yamaguchi, and S. A. Shivashankar, AIP Adv **10**, 015101 (2020).
[18]B. Reeja-Jayan, K. L. Harrison, K. Yang, C.-L. Wang, a. E. Yilmaz, and A. Manthiram, Sci. Rep. **2**, 1003 (2012).
[19]S. W. da Silva, F. Nakagomi, M. S. Silva, A. Franco, V. K. Garg, A. C. Oliveira, and P. C. Morais, J. Nanoparticle Res. **14**, 798 (2012).
[20]J. Smit and H. P. J. Wijn, *Ferrites* (N. V. Philips's Gloeiampenfabrieken, Eindhoven, 1959).
[21]M. Hu, J. Xu, J. Gao, S. Yang, J. S. P. Wong, and R. K. Y. Li, J. Chem. Soc. Dalt. Trans. **42**, 9777 (2013).
[22]V. H. Ojha and K. M. Kant, Phys. B Condens. Matter **567**, 87 (2019).
[23]T. N. Shendruk, R. D. Desautels, B. W. Southern, and J. Van Lierop, Nanotechnology **18**, 455704 (2007).
[24]K. Maaz, A. Mumtaz, S. K. Hasanain, and M. F. Bertino, J. Magn. Magn. Mater. **322**, 2199 (2010).
[25]K. Mandal, S. Mitra, and P. A. Kumar, Europhys. Lett. **75**, 618 (2006).
[26]S. V. Andreev, M. I. Bartashevich, V. I. Pushkarsky, V. N. Maltsev, L. A. Pamyatnykh, E. N. Tarasov, N. V. Kudrevatykh, and T. Goto, J. Alloys Compd. **260**, 196 (1997).
[27]E. C. Devi and I. Soibam, J. Alloys Compd. **772**, 920 (2019).
[28]Y. Shiratsuchi and M. Yamamoto, Phys. Rev. B **76**, 144432 (2007).
[29]D. Peddis, F. Orrù, A. Ardu, C. Cannas, A. Musinu, and G. Piccaluga, Chem. Mater. **24**, 1062 (2012).
[30]L. Néel, Proc. Phys. Soc. Sect. A **65**, 869 (1952).
[31]D. Peddis, C. Cannas, A. Musinu, and G. Piccaluga, J. Phys. Chem. C **112**, 5141 (2008).
[32]J. L. Dormann, L. Spinu, E. Tronc, J. P. Jolivet, F. Lucari, F. D'Orazio, and D. Fiorani, J. Magn. Magn. Mater. **183**, 255 (1998).